

# PHYSICAL REVIEW D

## PARTICLES AND FIELDS

THIRD SERIES, VOLUME 26, NUMBER 11

1 DECEMBER 1982

### Measurement of the neutral-current-to-charged-current cross-section ratio for antineutrino-proton inclusive scattering

D. D. Carmony, T. S. Carman,\* V. E. Barnes, C. Davis, E. Fernandez,<sup>†</sup>  
A. F. Garfinkel, and A. T. Laasanen  
*Purdue University, W. Lafayette, Indiana 47907*

M. Derrick, P. Gregory,<sup>‡</sup> F. LoPinto,<sup>§</sup> B. Musgrave, J. Schlereth, P. Schreiner,<sup>§</sup> and R. Singer<sup>§</sup>  
*Argonne National Laboratory, Argonne, Illinois 60439*

S. J. Barish,\*\* R. Brock,<sup>††</sup> A. Engler, T. Kikuchi, R. W. Kraemer, F. Messing,  
B. J. Stacey,<sup>††</sup> and M. Tabak\*  
*Carnegie-Mellon University, Pittsburgh, Pennsylvania 15213*

(Received 22 February 1982)

The Fermilab wide-band antineutrino beam incident on the hydrogen-filled 15-foot bubble chamber was used to study  $\bar{\nu}p$  neutral-current interactions. The  $u = x(1-y)$  distribution is presented for both the neutral- and the charged-current data sample. Fitting the neutral-current  $u$  distribution to the prediction of a simple quark-parton model measures the Weinberg angle. By using recent measurements of the neutral-to-charged-current cross-section ratio for  $\nu p$  interactions ( $R_p$ ), we find the corresponding ratio for  $\bar{\nu}p$  interactions ( $\bar{R}_p$ ) to be  $0.36 \pm 0.06$ .

### I. INTRODUCTION

Since the discovery of strangeness-conserving neutral-current interactions in 1973,<sup>1</sup> many different reactions mediated by the neutral current have been studied. All data<sup>2</sup> are now in agreement with the simple  $SU(2) \times U(1)$  model of Weinberg and Salam; and so the current analysis of our experiment is done in the context of this model. The fundamental parameter of the model, the Weinberg angle  $\theta_W$ , can be determined from the ratio of the inclusive neutral-current to charged-current cross sections. The most precise measurement of this quantity comes from experiments studying  $\nu$  and  $\bar{\nu}$  interactions on isoscalar targets, and they, together with other measurements,<sup>3</sup> give a value for the Weinberg angle of  $\sin^2 \theta_W = 0.232 \pm 0.009$ .

Four groups<sup>4</sup> have reported measurements of the inclusive neutral-current-to-charged-current cross-section ratio  $R_p$  for  $\nu p$  scattering, and the mean of these measurements is  $0.502 \pm 0.027$ . Apart from an early result from the present experiment<sup>5</sup> of  $\bar{R}_p = 0.42 \pm 0.13$ , no other inclusive  $\bar{\nu}p$  data are available. In this paper, we present our final results based on a data sample about four times larger than

that of Ref. 5. As a result of our analyses of other reactions, we now have a more detailed understanding of the problems of classifying the events and thus of the crucially important systematic errors.

No experiment has as yet measured the complete differential distribution  $d^2\sigma/dx dy$  for neutral-current interactions. Because of the missing lepton in the final state, broad-band neutrino/antineutrino experiments are unable to measure either of the usual scaling variables,  $x = Q^2/2M(E_{\bar{\nu}} - E'_{\bar{\nu}})$  or  $y = (E_{\bar{\nu}} - E'_{\bar{\nu}})/E_{\bar{\nu}} \approx E_H/E_{\bar{\nu}}$ , where  $E_{\bar{\nu}}$  and  $E'_{\bar{\nu}}$  are the energies of the initial and final  $\bar{\nu}$ , respectively, and  $E_H$  is the energy of the final hadronic system. Calorimetric experiments using narrow-band beams have, however, measured neutral-current  $y$  distributions.<sup>6</sup> Here we analyze our neutral-current interactions in terms of the variable  $u = x(1-y)$ . This variable depends only on the hadronic system since at high energy

$$u \approx p_H \theta_H^2 / 2M, \quad (1)$$

where  $p_H$  is the total hadronic momentum and  $\theta_H$  is the angle between the beam direction and the hadronic momentum vector. Since large bubble chambers measure both momenta and angles of

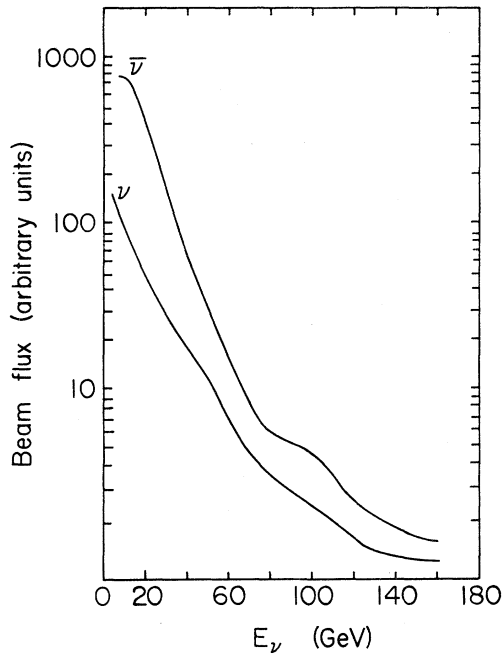


FIG. 1. Shapes and relative intensities of the  $\nu$  and  $\bar{\nu}$  fluxes as determined from the charged-current event energy distributions and assuming a linear cross section rise with energy.

charged particles very precisely, and the corrections needed for the missing neutral particles have been extensively studied, the  $u$  distribution is rather well determined.

## II. EXPERIMENTAL DETAILS

The data were obtained from 208 000 pictures of the hydrogen-filled 15-foot bubble chamber exposed to the wide-band antineutrino beam at Fermilab. About 90% of the pictures were taken using a 400-GeV/ $c$  proton beam.<sup>7</sup> A significant neutrino background is present in the beam as shown by the flux distributions of Fig. 1. In scanning the film, we only recorded events with three or more prongs. One-prong events were not recorded due to the high background of straight-through muon tracks. Measurement and reconstruction of the events were car-

ried out using standard techniques<sup>7</sup> and the overall pass rate, which was multiplicity dependent, was typically 90%. Corrections for the scanning and reconstruction inefficiencies were applied and are tabulated in Table I.

## III. EVENT CLASSIFICATION

The observed interactions must be assigned to one of the five categories:

$$\bar{\nu}p \rightarrow \mu^+ X^0 \text{ (}\overline{\text{CC}}\text{)}, \quad (2)$$

$$\bar{\nu}p \rightarrow \bar{\nu} X^+ \text{ (}\overline{\text{NC}}\text{)}, \quad (3)$$

$$\nu p \rightarrow \mu^- X^{++} \text{ (CC)}, \quad (4)$$

$$\nu p \rightarrow \nu X^+ \text{ (NC)}, \quad (5)$$

$$hp \rightarrow HNX \text{ (HB)}. \quad (6)$$

In order to make these assignments, cuts must be applied to the experimental data. First the hadron-induced background (HB) must be removed and then the neutrino events must be classified as CC,  $\overline{\text{CC}}$ , or (NC +  $\overline{\text{NC}}$ ). Reactions (2) and (4) are signed by the presence of the muon in the final state. We, of course, have no way of assigning the neutral-current events to reactions (3) or (5) separately, but the number of neutrino-induced neutral-current events can be determined since  $R_p$  has been measured.<sup>4</sup>

The purity and efficiency of the neutrino-induced data samples are measured by applying the cuts to a large Monte Carlo generated "data sample" and calculating  $x$ - and  $y$ -dependent correction factors. These correction factors are then applied to the experimental data to compensate for the effects of the cuts including misidentification of muons as hadrons. Our Monte Carlo program includes all the  $\nu$ - and  $\bar{\nu}$ -induced reactions and takes into account the different charge states of the hadronic system, the measured variation of charged and neutral multiplicity with  $W$ , the c.m. energy, and the  $P_{\text{vis}}$ , as well as the prong cut applied to the hadronic system. The program incorporates the Field and Feynman parton densities<sup>8</sup> and the Weinberg-Salam couplings<sup>9</sup>

TABLE I. Scanning and reconstruction efficiency for all events.

Prong count	No. of events recorder	Single-scan efficiency	Reconstruction efficiency	No. of NC + $\overline{\text{NC}}$ events with $P_{\text{vis}} > 5$ GeV/ $c$
3	5399	(79±4)%	96%	203
5	2068	(93±2)%	95%	323
7	752	(93±4)%	93%	139
9	258		89%	49
> 11	74		83%	11

for the neutral current. A detailed description of the Monte Carlo program is given in Appendix 3 of Ref. 7.

In determining the flux of Fig. 1, the data were constrained to give cross sections rising linearly with energy. The  $\bar{\nu}$  content of the beam was measured to be  $(83.3 \pm 1.8)\%$ .

### A. Hadronic background

In addition to the neutrinos that traverse the bubble chamber, there is a small flux of incident neutral hadrons ( $h$ ). These hadrons come predominantly from neutrino interactions in the muon shield and so are of lower energies than the primary neutrinos. The interaction of these hadrons in the bubble chamber gives events that are superficially similar to the NC neutrino interactions since in the latter reactions, the outgoing neutrino takes a large fraction of the event energy.

We find that neutron interactions can be effectively eliminated by requiring that the total visible

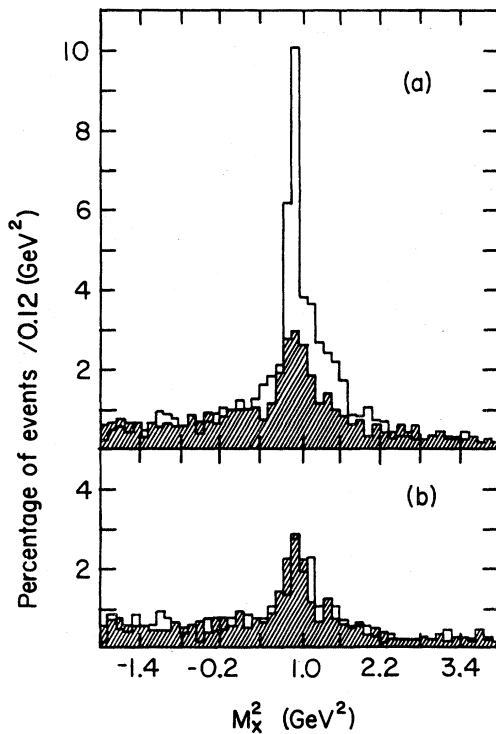


FIG. 2. The open histogram shows the distribution in the square of the beam mass  $M_x^2$  for three-prong events interpreted as the reaction  $xp \rightarrow pp\pi^-$ . (a) all events, (b) events with  $P_{\text{vis}} > 5$  GeV/c. The cross-hatched histograms are the same distributions for the MC-generated events.

momentum  $P_{\text{vis}}$  be greater than 5 GeV/c. We demonstrate the effectiveness of this cut in two ways. First, all of the three-prong events were interpreted as the reaction  $xp \rightarrow pp\pi^-$  and energy and momentum constraints were used to calculate the mass squared of  $x$ ,  $M_x^2$ . The  $M_x^2$  variation is compared in Fig. 2(a) with the distribution predicted by our Monte Carlo (MC) simulation program, shown as the cross-hatched histogram. The comparison is shown again in Fig. 2(b) after making the cut  $P_{\text{vis}} > 5$  GeV/c. The clear excess of events over the MC prediction at the neutron mass in Fig. 2(a) completely disappears after the 5-GeV/c momentum cut. The enhancement near  $M_x^2 = 1$  GeV/c in both the data and the MC distribution is entirely understood as stemming from events such as  $\bar{\nu}p \rightarrow \mu^+ p\pi^-$  or  $\nu p \rightarrow \mu^- p\pi^+$  being misinterpreted as neutron interactions.

The second analysis of the neutron background is based on the fact that a significant fraction of the total cross section for  $np$  scattering results in a forward, diffractively produced  $p\pi^-$  system, which predominantly has  $M_{p\pi} < 1.7$  GeV. We have calculated the effective mass of the fastest positive and negative tracks in each event. In Fig. 3, we compare the frequency of events having  $M_{p\pi} < 1.7$  GeV in the event sample with that from the Monte Carlo

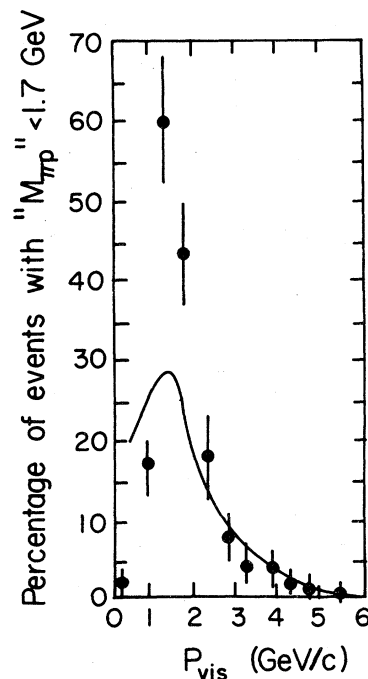


FIG. 3. Fraction of events with " $M_{np}$ "  $< 1.7$  GeV as a function of  $P_{\text{vis}}$  for all the events.  $M_{np}$  is calculated from the fastest positive and negative track as discussed in the text. The curve is the Monte Carlo prediction.

sample as a function of  $P_{\text{vis}}$ . For low  $P_{\text{vis}}$ , a neutron-induced excess is clearly evident, but for  $P_{\text{vis}} > 2.5$  GeV/c, the shapes of the two distributions agree quite well.

We have previously<sup>5</sup> attempted to measure the  $K_L^0$  flux by kinematically fitting all the multivertex events. No acceptable fits to  $K_L^0 p$  interactions with  $K_L^0$  momenta above 2 GeV/c were found. Recently, we have measured the momentum spectrum of the strange particles produced in this experiment<sup>10</sup> and estimate that the total background due to the upstream production of beamlike  $K_L^0$  is less than four events after the  $P_{\text{vis}} > 5$  GeV/c cut is applied.

We conclude that the total hadronic-background correction is negligible for events having a momentum sum of the charged hadrons greater than 5 GeV/c.

### B. Classification of events

Having removed the hadronic background by the visible-momentum cut, it remains to classify the events as either antineutrino charged current ( $\overline{\text{CC}}$ ), neutrino charged current (CC), or as neutral current ( $\overline{\text{NC}} + \text{NC}$ ).

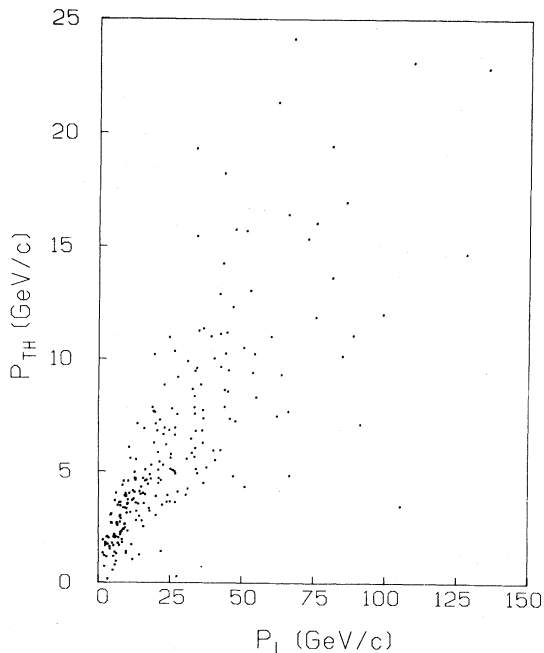


FIG. 4. Scatter plot of  $P_{TH}$  vs  $P_L$  for kinematically selected  $\mu^\pm$  tracks.  $P_L$  is the laboratory momentum of the selected track in the beam direction and  $P_{TH}$  is the transverse component of the selected track relative to the hadronic direction defined as the vector sum of the momenta of all the charged tracks except the selected muon.

We select the muons using a kinematical method which is detailed in our recent study of the  $\overline{\text{CC}}$  events.<sup>11</sup> The kinematical selection method is based on two observed properties of the produced hadrons. First, the hadrons have a limited transverse momentum with respect to the hadronic direction, typically  $P_{TH} \lesssim 0.4$  GeV/c, and second, the hadronic tracks are predominantly produced at small values of Feynman  $x_F$  and thus have moderate momenta in the laboratory frame.<sup>12</sup> On the other hand, especially in antineutrino interactions, the outgoing lepton tends to carry a large fraction of the incident momentum and since the average four-momentum transfer squared ( $\langle Q^2 \rangle$ ) is about 4.4 (GeV/c)<sup>2</sup>, the muon generally has a large component of momentum perpendicular to the hadronic direction. Figure 4 shows a scatter plot of  $P_{TH}$  vs  $P_L$  for those tracks kinematically selected as muons for a subsample of our data. The quantity  $P_{TH}$  is the component of the momentum of the selected track perpendicular to the direction defined by the vector sum of the momentum of all the *charged* tracks except the kinematically selected muon. The quantity  $P_L$  is the momentum component of the selected track in the beam direction. Figure 5 shows the same scatter plot for each of the other

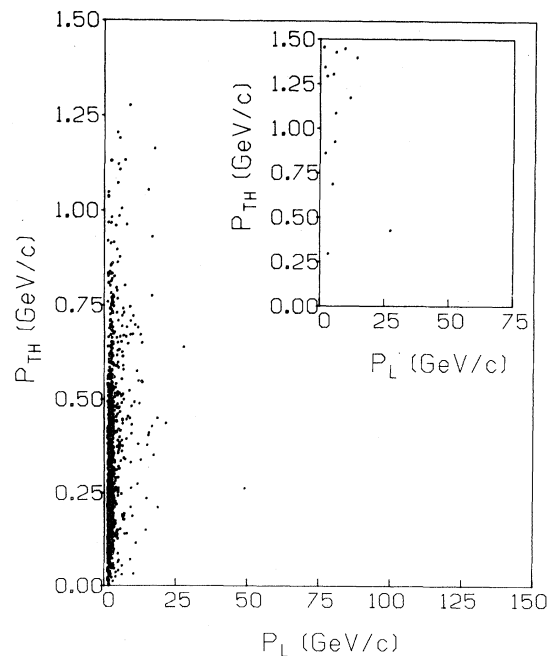


FIG. 5. Scatter plot of  $P_{TH}$  vs  $P_L$  (defined in Fig. 4) for the individual hadrons in kinematically selected charged current ( $\overline{\text{CC}} + \text{CC}$ ) events. Note the expanded vertical scale as compared to Fig. 4. The insert shows the muon data over the same kinematic range.

TABLE II. Kinematic  $P_{TH}$  and  $P_L$  for hadron and muon tracks.

Event class	Muon		Hadron	
	$\langle p_{TH} \rangle$	$\langle p_L \rangle$	$\langle p_{TH} \rangle$	$\langle p_L \rangle$
	(GeV/c)		(GeV/c)	
$\bar{\nu}p: \overline{CC}$	5.8	21.0	0.34	2.2
$\nu p: CC$	5.1	26.7	0.40	3.9
$\overline{NC} + NC$			0.42	3.7

tracks in the events classified as  $\overline{CC}$  or  $CC$  events. Note that the vertical scale has been greatly expanded. The data of Fig. 4 are shown on the same expanded scale as an inset. As can be seen from these figures and in Table II, the typical  $\overline{CC}$  event has one track with  $\langle P_{TH} \rangle = 5.8$  GeV/c and  $\langle P_L \rangle = 21$  GeV/c, whereas the remaining tracks have mean values of  $\langle P_{TH} \rangle = 0.34$  GeV/c and  $\langle P_L \rangle = 2.2$  GeV/c. The kinematical method works because of these major differences between the kinematics of the muon and those of the hadrons. Figure 6 shows the scatter plot  $P_{TH}$  vs  $P_L$  for the tracks from a subsample of events classified as neutral current ( $NC + \overline{NC}$ ). These tracks are seen to have a distribution very similar to that of the hadrons in the  $CC + \overline{CC}$  events (Fig. 5) and totally unlike that of the muons.

The muon algorithm used was thus as follows: We define forward events to be those in which all tracks have transverse momentum with respect to the beam direction less than 1.0 GeV/c. Forward events are selected as charged current events if the ratio of the highest to the next highest track momentum is greater than 2.0. The highest-momentum track is then identified as the muon. The nonforward events are selected as charged current if any track has a transverse momentum greater than 1.3 GeV/c with respect to the total momentum direction of the remaining charged tracks. The largest transverse momentum track is then identified as the muon. The charge of the selected muon track classifies the event as being  $\nu$ - or  $\bar{\nu}$ -induced. Where no muon can be selected, the event is classified as neutral current ( $NC + \overline{NC}$ ).

Using MC-generated events, we can determine the efficiency  $\epsilon_i$  of the kinematic selection algorithm. This is defined as that fraction of the events generated as type  $i$  which are correctly classified as type  $i$  (with the correct track classified as a muon in the case of a charged-current event), after making the appropriate cuts. We can also determine the backgrounds  $b_i$ , defined as the number of events incorrectly classified as type  $i$ , divided by the total number of events classified as type  $i$ . The efficien-

cies and backgrounds for the  $\overline{CC}$ ,  $CC$ , and ( $\overline{NC} + NC$ ) samples are given in Table III from which it is evident that the ( $\overline{NC} + NC$ ) sample has the lowest efficiency and the highest background.

For those events which are classified as charged current, we have checked the sample purity. Those tracks which are kinematically selected as muons were examined for visible secondary hadronic interactions in the bubble chamber. From a study of a sample of such interactions, the background in the  $\overline{CC}$  sample is  $8 \pm 3\%$ , which is in agreement with the Monte Carlo background estimate of  $7\%$ .<sup>13</sup>

Our Monte Carlo studies indicate that if we could restrict ourselves to a limited kinematical region of the scaling variables, namely,  $x > 0.05$  and  $y < 0.8$ , we would select all classes of events with

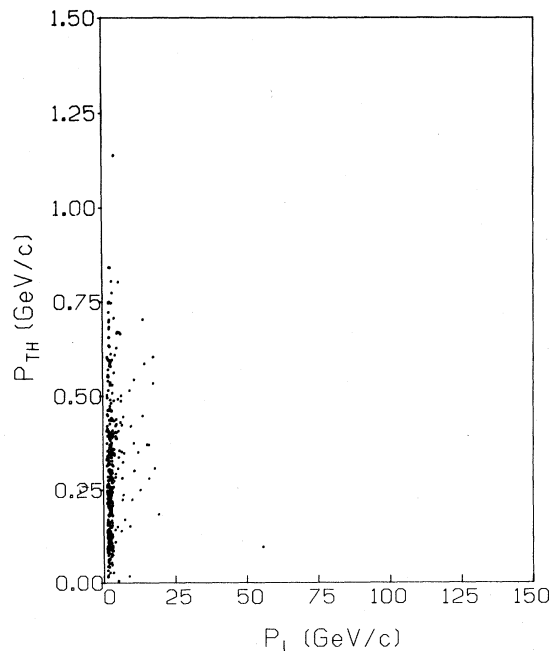


FIG. 6. Scatter plot of  $P_{TH}$  vs  $P_L$  for the individual tracks from events kinematically selected as NC interactions. Here the hadronic direction is defined as the vector sum of the momenta or all the charged tracks. Figs. 4-6 are shown for the same subsample of the film.

TABLE III. Monte Carlo estimates of selection efficiencies and backgrounds.

Event class	Entire kinematic region		$u > 0.06$	
	Efficiency $\epsilon_i$	Background $b_i$	Efficiency $\epsilon_i$	Background $b_i$
$\bar{\nu}p: \bar{CC}$	0.89	0.17	0.97	0.07
$\nu p: CC$	0.82	0.23	0.91	0.07
$\bar{NC}+NC$	0.62	0.30	0.93	0.20

better efficiency and reduced background. In the excluded region of small  $x$  and large  $y$ , i.e., large energy transfer, the outgoing lepton tends to be of low momentum and thus fails to be separated from the hadrons. While such kinematic cuts were indeed made in our charged-current analysis,<sup>7</sup> rather large corrections for charged-current contamination of the neutral-current sample were needed in our previous determination<sup>5</sup> of  $\bar{R}_p$  since neither  $x$  nor  $y$  is measurable for NC events in a broad-band beam.

Although we cannot determine  $x$  and  $y$  individually, the quantity  $u = x(1-y)$  which, as seen from Eq. (1), depends only on the vector momentum of the hadronic system is fairly well measured even in a hydrogen bubble chamber where a correction for neutral hadronic energy is necessary. These corrections are made via the MC simulation and are described in detail in the Appendix of Ref. 7. The resulting uncertainty in  $u$  is typically 0.025 (0.04) for the charged-current (neutral-current) events and decreases as  $u$  decreases.

The selection  $u > 0.06$  approximately simulates the  $x$  and  $y$  cuts discussed previously, as seen in Fig. 7. We henceforth apply the  $u > 0.06$  cut to both the

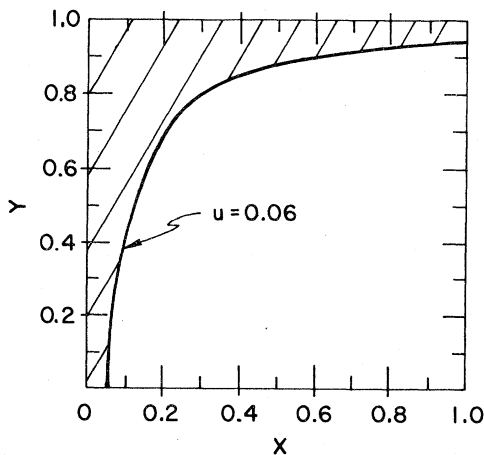


FIG. 7. The allowed kinematic region in  $x$  and  $y$  with a selection  $u = x(1-y) > 0.06$ . The shaded area is excluded.

charged- and neutral-current samples. As is seen in Table III, this increases the efficiency and reduces the background for all classes of events.

#### IV. RESULTS

Figure 8 shows the calculated  $u$  distribution  $dN/du$  for the  $\bar{CC}$  and  $CC$  events, as well as that predicted for our mixture of  $(\bar{NC} + NC)$  events for several values of the Weinberg angle. The predicted  $u$  distributions for values of  $\sin^2\theta_w$  in the range 0.1 to 0.5 are quite similar. The only other free parameter is one overall normalization which we obtain by area normalizing the  $\bar{CC}$  data to the calculated  $u$  distribution. Figure 9(a) shows this  $u$  distribution with the best-fit curve. Figure 9(b) shows the same distribution for the  $CC$  events. Fitting the  $(\bar{NC} + NC)$   $u$  distribution of Fig. 9(c) to the data gives two solutions for the Weinberg angle. These are  $\sin^2\theta_w = 0.13^{+0.08}_{-0.05}$  and  $\sin^2\theta_w = 0.50^{+0.05}_{-0.09}$ . The

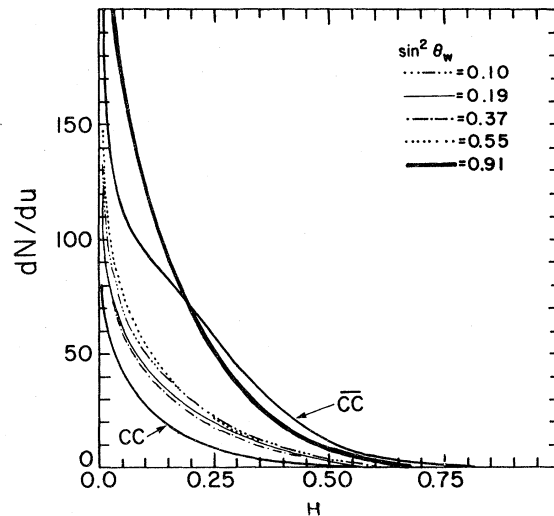


FIG. 8. The differential cross section  $dN/du$  for  $\bar{\nu}p \rightarrow \bar{CC}$ ,  $\nu p \rightarrow CC$  events compared to the distributions for our mixture of  $\bar{NC} + NC$  events using several values of the Weinberg angle. The predictions, which include our flux distributions and experimental cuts, are relative-normalized for a beam which is 83.3%  $\bar{\nu}$ .

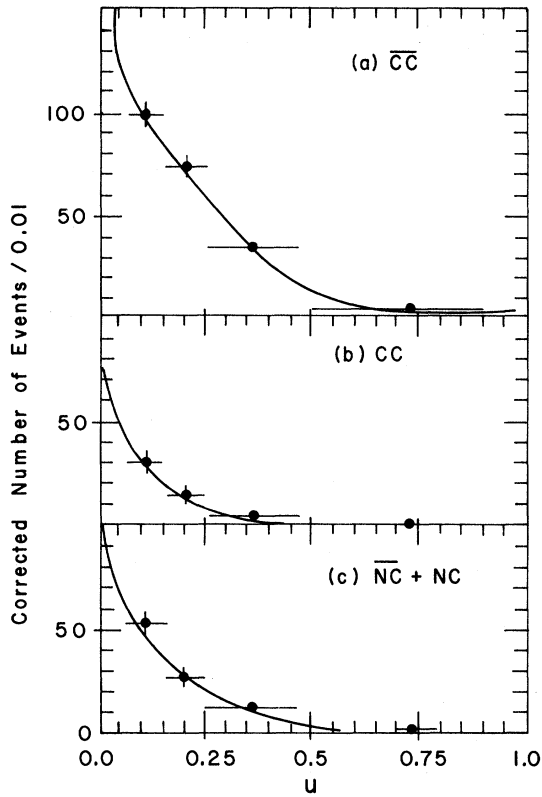


FIG. 9. Experimental differential cross sections  $dN/du$  for (a) the  $\overline{CC}$ , (b) the  $CC$ , and (c) the  $\overline{NC} + NC$  events, all for  $u > 0.06$ . Only the curve for the  $\overline{CC}$  case is area-normalized to the data.

first solution is compatible with the average value obtained from other experiments, and these in turn rule out the second solution.

A measurement of  $\overline{R}_p$ , the ratio of neutral-current to charged-current total cross sections in  $\overline{\nu p}$  interactions, can be combined with the published ratio  $R_p$  for  $\nu p$  interactions to give another measure of the Weinberg angle. Using the world-average value of  $R_p = 0.502 \pm 0.027$  to subtract off the  $\nu p$  events from our total neutral-current data, we obtain  $\overline{R}_p = 0.36 \pm 0.04$  where the error is a combination of our statistical uncertainty and the error on  $R_p$ . In calculating  $\overline{R}_p$ , we have used the Weinberg-Salam model to repopulate the region  $u < 0.06$ . From repeated Monte Carlo runs with varying parametrizations, we conclude that a total systematic error of  $\pm 0.04$  is appropriate. Thus our combined error is  $\pm 0.06$ . Figure 10 shows our result on an  $\overline{R}_p$  vs  $R_p$  plot, together with the locus of the expected points as  $\sin^2\theta_W$  is varied. The combined data point is within one standard deviation of the expected locus, and the combination of the  $\nu p$  and  $\overline{\nu p}$  experiments measure  $\sin^2\theta_W$  to be  $0.19 \pm 0.05$ .

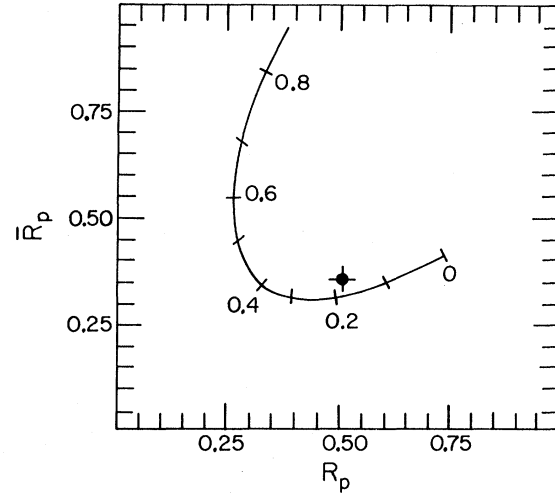


FIG. 10. Measured value of  $\overline{R}_p$  (this experiment) vs the world-average value for  $R_p$  (Ref. 4). The curve is the Weinberg-Salam prediction with values of  $\sin^2\theta_W$  indicated, calculated using the parton densities of Field and Feynman (Ref. 8).

## V. CONCLUSIONS

We have measured the ratio of the total cross section for neutral currents to that of charged currents in  $\overline{\nu p}$  interactions,  $\overline{R}_p$ , to be  $0.36 \pm 0.06$ . This value, combined with the value of  $R_p$  from  $\nu p$  interactions, measures the Weinberg angle to be  $\sin^2\theta_W = 0.19 \pm 0.05$  in good agreement with the world average of  $0.232 \pm 0.009$ . We have also measured the Weinberg angle using the distribution  $d\sigma/du$ , where  $u$  is given in terms of the usual scaling variables by  $u = x(1-y)$  and find  $\sin^2\theta_W = 0.13^{+0.08}_{-0.05}$ . These  $dN/du$  measurements, though limited in statistics, when taken with earlier measurements of  $d\sigma/dy$  for neutral currents indicate that the Weinberg-Salam model not only correctly predicts the rate of the neutral-current interaction but also the double-differential cross section  $d^2\sigma/dx dy$ .

## ACKNOWLEDGMENTS

This experiment was made possible by the support of the Fermilab Neutrino Department and, in particular, the operating crew of the 15-foot bubble chamber. We also wish to thank our scanners at all three institutions for their careful job. Finally, we acknowledge the communication and discussion of results on neutral current studies in  $\nu p$  interactions by T. Kafka. This work was supported by the U. S. Department of Energy.

- \*Present address: Lawrence Livermore Laboratory, Livermore, CA 94550.
- †Present address: Argonne National Laboratory, Argonne, IL 60439.
- ‡Present address: CERN, EP Division, Geneva 23, Switzerland.
- §Present address: Bell Telephone Laboratories, Naperville, IL 60540.
- \*\*Present address: U.S. Department of Energy, Washington, D.C. 20545.
- ††Present address: Fermi National Accelerator Laboratory, Batavia, IL 60510.
- ‡‡Present address: University of Toronto, Toronto, Ontario, Canada.
- <sup>1</sup>F. J. Hasert *et al.*, Phys. Lett. **46B**, 138 (1973).
- <sup>2</sup>See the recent review talk by F. Büsser, in *Neutrino 81*, Proceedings of the International Conference on Neutrino Physics and Astrophysics, Maui, Hawaii (1981), edited by R. J. Cence, E. Ma, and A. Roberts (University of Hawaii High Energy Physics Group, Honolulu, 1981), Vol. 2, p. 351.
- <sup>3</sup>J. E. Kim *et al.*, Rev. Mod. Phys. **53**, 211 (1981).
- <sup>4</sup>The two published measurements of  $R_p$  are  $0.48 \pm 0.17$  by F. J. Harris *et al.*, [Phys. Rev. Lett. **39**, 437 (1977)] and  $0.51 \pm 0.04$  by J. Blietschau *et al.* [Phys. Lett. **88B**, 381 (1979)]. In addition, two other experiments have reported values:  $R_p = 0.47 \pm 0.05$  [T. Kafka *et al.*, in *Neutrino 81* (Ref. 2), Vol. 2, p. 363] and  $R_p = 0.53 \pm 0.055$  [V. Brisson *et al.*, in *Neutrino 81* (Ref. 2), Vol. 2, p. 129].
- <sup>5</sup>M. Derrick *et al.*, Phys. Rev. D **18**, 7 (1978).
- <sup>6</sup>M. Jonker *et al.*, Phys. Lett. **102B**, 67 (1981).
- <sup>7</sup>The experimental details, including a description of the Monte Carlo simulation, are given in V. E. Barnes *et al.*, Phys. Rev. D **25**, 1 (1982).
- <sup>8</sup>R. D. Field and R. P. Feynman, Phys. Rev. D **15**, 2590 (1977).
- <sup>9</sup>J. Goldstone, A. Salam, and S. Weinberg, Phys. Rev. **127**, 3 (1962).
- <sup>10</sup>R. Brock *et al.*, Phys. Rev. D **25**, 1753 (1982).
- <sup>11</sup>A detailed discussion of the muon-selection algorithm is given in an appendix to Ref. 7. See also E. Fernandez, Ph.D. thesis, Purdue University, 1979 (unpublished); T. S. Carman, Ph.D. thesis, Purdue University, 1981 (unpublished).
- <sup>12</sup>M. Derrick *et al.*, Phys. Rev. D **24**, 1071 (1981). The transverse and longitudinal hadron distributions are shown in Figs. 14 and 9, respectively.
- <sup>13</sup>Furthermore, during the exposure an external muon identifier (EMI), a series of wire chambers, was operated downstream of the bubble chamber and behind several nuclear interaction lengths of absorber. Because the geometric acceptance times the fraction of the time the EMI was operational was low, and because the then operating EMI had an inadequate absorber and shielding, we were unable to extract muon identification on a track-by-track basis. Nevertheless, the analysis of the EMI data on a statistical basis confirms the correctness of our measurement of the  $\mu^\pm$  purity.